GOFOS, ground optical fog observation system for monitoring the vertical stratocumulus-fog cloud distribution in the coast of the Atacama Desert, Chile

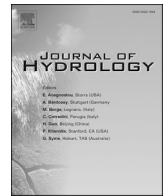Río, Camilo; Lobos, Felipe; Siegmund, Alexander; Tejos, Cristian; Osses, Pablo et al

Research papers

GOFOS, ground optical fog observation system for monitoring the vertical stratocumulus-fog cloud distribution in the coast of the Atacama Desert, Chile

Camilo del Río [a,b,*], Felipe Lobos [c,d], Alexander Siegmund [e,f], Cristian Tejos [g], Pablo Osses [a,b], Zeidy Huaman [c], Juan Pablo Meneses [g], Juan-Luis García [a,b]

[a] Pontificia Universidad Católica de Chile, Instituto de Geografía, Santiago, Chile
[b] Centro UC Desierto de Atacama, Santiago, Chile
[c] Pontificia Universidad Católica de Chile, Departamento de Ingeniería Hidráulica y Ambiental, Santiago, Chile
[d] Meteorology and Air Quality Group, Wageningen University, Wageningen, The Netherlands
[e] Heidelberg Center for the Environment & Institute for Geography, Heidelberg University, Heidelberg, Germany
[f] Research Group for Earth Observation (rgeo), Department of Geography, Heidelberg University of Education, Heidelberg, Germany
[g] Pontificia Universidad Católica de Chile, Department of Electrical Engineering, Biomedical Imaging Center and Millennium Nucleus for Cardiovascular Magnetic Resonance, Chile

ARTICLE INFO

ABSTRACT

Studying fog requires a good understanding of both its horizontal and vertical distributions. Among these two, the vertical one is the most challenging to observe. Different methods have been adopted for observing this variable, among which the most commonly used are satellite datasets, together with airborne and meteorological surface observations. Yet, all these techniques present significant limitations as for spatial and temporal resolution when describing the vertical fog structure. In this manuscript, we introduce the Ground Optical Fog Observation System (GOFOS), a new method to describe the advective fog's frequency and vertical distribution. This tool is based on in-situ optical observations, taking advantage of the topography of the Atacama Desert coastal mountains, where advective fog is frequent. During 2017, the GOFOS reported a fog presence <10% during summer and of ~50% during winter. Also, the GOFOS shows a diurnal variability of fog presence that decreases around noon and increases again starting from the afternoon. The vertical structure observed by the GOFOS shows a cloud depth of ~250 m, subject to diurnal and seasonal variabilities. By analyzing GOFOS results through a comparison with the ones obtained by standard observations, a ~93% agreement was found between the fog frequencies detected by the GOFOS and GOES. Also, we found a ~80% consistency between GOFOS fog frequency values and marine boundary layer regimes related to fog formation. Moreover, we observed that the cloud base height estimated by the GOFOS is correlated with the Iquique Airport ceilometer measurements (r = +0.6). Finally, the mean cloud top height estimated by the GOFOS differs by 8% from the Antofagasta Airport radio-soundings measurements. These results provide useful information for the selection of optimal sites for fog harvesting and for getting a better understanding of the interactions between fog and its ecosystem. In conclusion, through this study the GOFOS demonstrated its potential as a simple, reliable, and affordable method for systematic fog monitoring that might also be adapted to different topographic conditions.

1. Introduction

Fog is a meteorological phenomenon defined by a dense boundary layer cloud in permanent contact with the Earth's surface (Roach, 1994; Stull, 1988). Different conditions of the atmospheric boundary layer can originate three types of fogs. Radiative fog forms from air masses cooling in contact with a cold surface under stable atmospheric conditions (Roach et al., 1976; Bruijnzeel et al., 2005). Orographic fog forms under steep terrain conditions, where air masses lift while cooling down (Cereceda et al., 2002). Likewise, the well-known marine stratocumulus

cloud deck forms large fog banks when interacting with higher enough reliefs, generating advective fog (Bruijnzeel et al., 2005). The variety of conditions in which fog occurs determines its worldwide distribution (Eugster, 2008; Klemm et al., 2012) and creates the opportunity for addressing it under different research perspectives. Fog studies have largely focused on the impact of fog on the development of certain economic activities associated with land and aerial transport (Bendix, 2002). More recently, the scientific community has focused on the study of fog as a potential untapped freshwater resource. This research field is becoming more and more relevant in relation to climate change studies, especially for water-stressed areas, as in the case of the coast of the Atacama Desert (18°–30°S, 71°W) (Schemenauer and Cereceda, 1994a; Larraín et al., 2002; Cereceda et al., 2008a; Klemm et al., 2012; Marzol, 2002; Marzol and Sánchez, 2008; del Río et al., 2018). On this coast, we mainly find the advective fog, formed as a result of the combination of three physical processes. Firstly, the subsidence of warm air related to the SE Pacific Anticyclone interacts with the cold, wet and well-mixed marine boundary layer (MBL) generating a thermal inversion layer (Cereceda et al., 2002, 2008a; Garreaud et al., 2008; Muñoz et al., 2016; Lobos et al., 2018; del Río et al., 2018). Secondly, the newly formed thermal inversion, enhanced by the long-wave radiative cooling, promotes the formation of semi-permanent stratocumulus (Sc) clouds in the SE Pacific Ocean (Duynkerke et al., 1995; Garreaud et al., 2008, 2011; Garreaud and Muñoz, 2004; Serpetzoglou et al., 2008). Finally, predominant S-SW winds transport the Sc cloud towards the coast of the Atacama Desert, where the cloud intercepts the coastal mountain. This interaction leads to the formation of advective fog, whose diurnal variability is strongly influenced by the ocean-land thermodynamics (Lobos et al., 2018; Rutllant et al., 2003; Muñoz et al., 2016).

The vertical structure of the Sc cloud has already been explored (Serpetzoglou et al., 2008; Bretherton et al., 2010; Rutllant and Garreaud, 2005; Garreaud et al., 2011; Muñoz et al., 2011, 2016; Rutllant et al., 2003). Conversely, less is known about Sc cloud distribution when interacting with the Coastal Cordillera topography, forming advective fog (Lobos et al., 2018; Cereceda et al., 2008a, 2008b). A better understanding of advective fog frequency and its vertical structure is important for detecting where the fog mostly occurs and for characterizing its diurnal evolution and seasonality. This knowledge is essential for localizing optimal sites for fog harvesting (Marzol, 2005; Schemenauer & Joe, 1989; Schemenauer & Cereceda, 1994b). Additionally, the presence of fog within the coast of the Atacama Desert supports a unique natural ecosystem, rich in biodiversity and endemism (Schulz et al., 2011a; Muñoz-Schick et al., 2001; Pinto et al., 2006; Koch et al., 2019). This ecosystem is particularly sensitive to environmental variations related to nutrient and water inputs that depend on the fog (Latorre et al., 2011). As a consequence, the knowledge of cloud vertical variations has a high conservation value. In this sense, we can conclude that fog frequency and vertical distribution are relevant in terms of climate change, biodiversity conservation, and freshwater sources (Larraín et al., 2002; Schulz et al., 2011b; Klemm et al., 2012).

The study of advective fog (or stratocumulus-fog cloud, "ScF" in this paper) as a potential freshwater source requires an accurate understanding of horizontal and vertical fog distribution. Among these, the vertical component is the most challenging variation to measure. This has been studied before by using different methods and combinations of them, namely satellite images, as well as surface and airborne observations (Gultepe et al., 2007).

The most frequently used method to obtain an ScF horizontal scale is the analysis of satellite images. On one hand, satellites optimally describe the seasonal and diurnal fog cycles, as well as fog frequency (Bendix, 2002; Farías et al., 2005; Torregrosa et al., 2015; del Río et al., 2018). On the other hand, the analysis of these images presents significant limitations in describing the fog vertical structure (Bendix et al., 2005; Cermark, 2007). As for the surface observations method (i.e. meteorological stations), this is more suitable for measuring local meteorological variables, allowing accurate site-specific

characterizations of fog with high temporal resolution. Yet, this method reveals its limitations when it comes to characterizing the vertical fog structure for extended areas. For example, a large number of weather stations, fog collectors, and cloud radars are needed for a regional-scale fog study (Schween et al., 2020), leading to increased economic costs.

Airborne observations are so far the best alternative for measuring the vertical structure of ScF clouds, although they present severe limitations in terms of temporal resolution, given that the vertical distribution of the ScF is very dynamic, thus losing accuracy in describing diurnal cycles. Moreover, the frequently used radiosoundings are typically launched from airports or flatlands, thus providing results that do not consider the influence of topography.

Within this paper, we propose a new method, called Ground Optical Fog Observation System (GOFOS), for measuring frequency and vertical components of the ScF while addressing some of the issues listed above. The results derived from the testing of this method have been validated through standard methods and observations. Thanks to this analysis, we could observe how the GOFOS combines the synchronous high temporal resolution of surface observations with vertical observations, taking advantage of the local topography. Through this study, we aim to answer the following question: how does the GOFOS perform characterizing the ScF frequency and its vertical structure?

The article is structured as follows: in Section 2, the GOFOS instrumentation and operation are described, together with the relative data processing; within Section 3, the results regarding ScF frequency and vertical distribution are shown; within Section 4, the GOFOS performance is analyzed by comparing its results with the ones obtained through standard methods; finally, in Section 5, the main conclusions of this study are presented, together with GOFOS potential future applications.

2. Materials and methods

2.1. GOFOS instrumentation and installation

The Ground Optical Fog Observation System (GOFOS) was installed in the Coastal Cordillera of the Atacama Desert, at 15 to 20 km from the coastline and between 600 and 1350 m above the sea level (asl), where advective fog can be found (Fig. 1A and B). The GOFOS is composed of two optical time-lapse cameras configured to acquire an image every 10 min, and a series of solar-powered lights that automatically activate in the dark. The cameras (Brinno proTLC) are installed on a plastic tripod and connected to a 10 W solar panel for getting continuous power supply (Fig. 1C). The light system is installed on a 1.5 m galvanized iron pole and it consists of 44 LEDs (configured in a red mode) supplied by a 6 W solar panel (Fig. 1D). The cameras are strategically placed in two sites: at 1350 m asl (20.580429°S, 70.029714°W), and at 600 m asl (20.627451°S, 70.058907°W). The choice of these specific locations permits the observation of both the top and the base of the stratocumulus clouds (Fig. 1B), covering the 750 m height range that corresponds to the area of Stratocumulus-fog (ScF) presence (Cereceda et al., 2008b). These cameras oversee a transect of pole-lights located every 50 m along the slope from 600 to 1350 m asl. The top camera frames from E to W (i.e., towards the Pacific Ocean) nine pole-lights located between 850 m and 1250 m asl. The bottom camera frames, from W to E, a profile of pole-lights installed between 650 m and 900 m asl. The observation of the well-defined fog day cycle, with higher frequencies during the afternoon, night and dawn (Cereceda et al., 2008a), is performed through different methods during night and day times. A night image showing lights indicates the absence of fog. Contrarily, assuming that lights can be covered by the fog itself, the same night image without lights shown indicates the presence of fog. As for day images, by taking into account the exact location and height of the pole-lights in the slope, it is possible to visually determine the presence or absence of ScF, as well as the level (height) of the cloud top (CT) and cloud base (CB). Moreover, if the cameras capture images composed of fog only (i.e. foggy blank images),
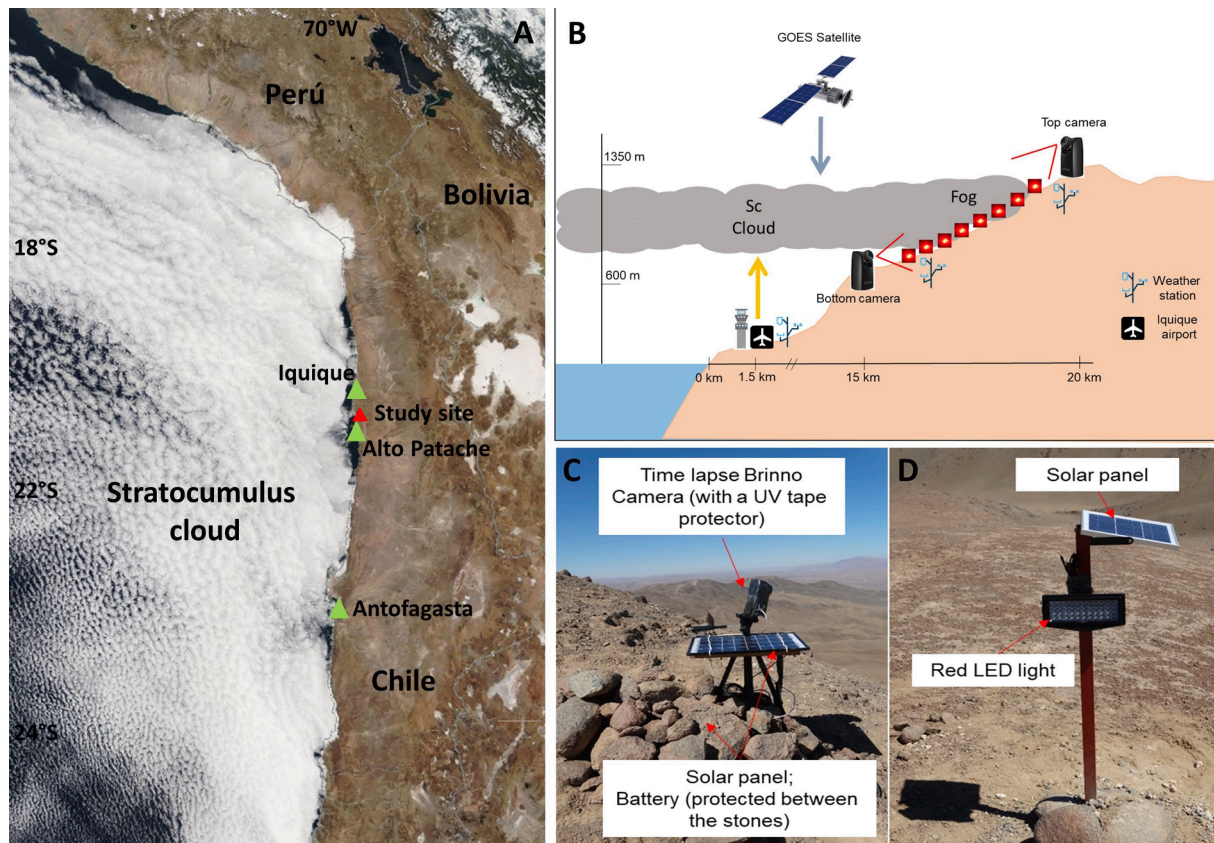
Fig. 1. Study field: A) Terra MODIS satellite image of the S-E Pacific Ocean and the Atacama Desert during a typical advective fog event, September 1st, 2019; B) vertical cross-section of GOFOS installation, together with the weather stations and ceilometer installed at Iquique Airport.; C) time-lapse camera; D) LED pole-lights.

ScF presence is recorded at the correspondent location and height. In summary, the cameras' observations indicate the Stratocumulus-fog cloud presence, the CT and CB heights, and the cloud depth (CD). The top camera captured images from August 2016 to January 2018, whereas the bottom one captured images from January 2017 to January 2018.

2.2. Data processing

Initially, a subset of 5080 pictures acquired by GOFOS cameras was manually processed to obtain a database of CT, CB, and CD measures. More specifically, the 5080 pictures were labeled by a supervisor who determined the presence or absence of fog for each sample. Additionally, pictures were manually classified as either night or day images. For the night ones, a binary classification was done by visual inspection of the pole-light elevation corresponding to each picture. According to this classification, the value 1, corresponding to non-visible light, indicates fog presence (Fig. 2B and D) and the value 0, corresponding to visible light, indicates fog absence, (Fig. 2A and C). The previous data subset was used to run a deep learning model based on a convolutional neural network, an algorithm that had already been successful used in several weather-image interpretation processes (Liu et al., 2016; Shi et al., 2016; Zhang et al., 2018). The model was run using the Python programming language (Python Software Foundation, https://www.python.org/) and an architecture based on the one proposed by Shi et al. (2016). The neural network received as input specific cropped regions of pictures where the pole-lights were located, returning as output the correspondent probability of fog presence. According to these outputs:

- If the probability was lower than 25%, no fog was detected.
- If the probability was higher than 75%, the fog was detected.

- If the probability was between 25% and 75%, the software let the user (supervisor) determine the presence or absence of fog.

After running the fully automated classification process the following quality statistics have been obtained:

$$Accuracy : \frac{Correct\ positives + Correct\ negatives}{Total\ observations} = 91.02\%$$

$$Specificity : \frac{Correct\ negatives}{Correct\ negatives + False\ Positives} = 92.91\%$$

$$Sensitivity : \frac{Correct\ positives}{Correct\ positives + False\ Negatives} = 80.53\%$$

In case of uncertainties (due to dimmed lights or lights interacting with cloud boundaries), the software was configured so that the user could manually classify the images (Fig. 2E and F), improving the algorithm's performance to avoid false negatives detections. Then, the binary results were automatically systematized into a database. The remaining pictures (nearly 32,000) were automatically classified by the model, whereas for daylight pictures, the entire binary classification was performed manually. Finally, diurnal and nocturnal datasets were unified. The presence of fog was confirmed if at least one of the observations (diurnal and nocturnal) corresponded to the binary value 1. This method was used to calculate the ScF frequency for a determined time-period (an hour, a day, or a month). For example, 50% of an hour of fog presence corresponds to 3 observations (taken every 10 min) reporting the value 1, 50% of a day of fog presence corresponds to 72 observations reporting the value 1, and 50% of a month of fog presence corresponds to 2160 measurements with value 1.

The heights of CT and CB were estimated through the highest and lowest synchronic fog observations, respectively. Finally, the CD was
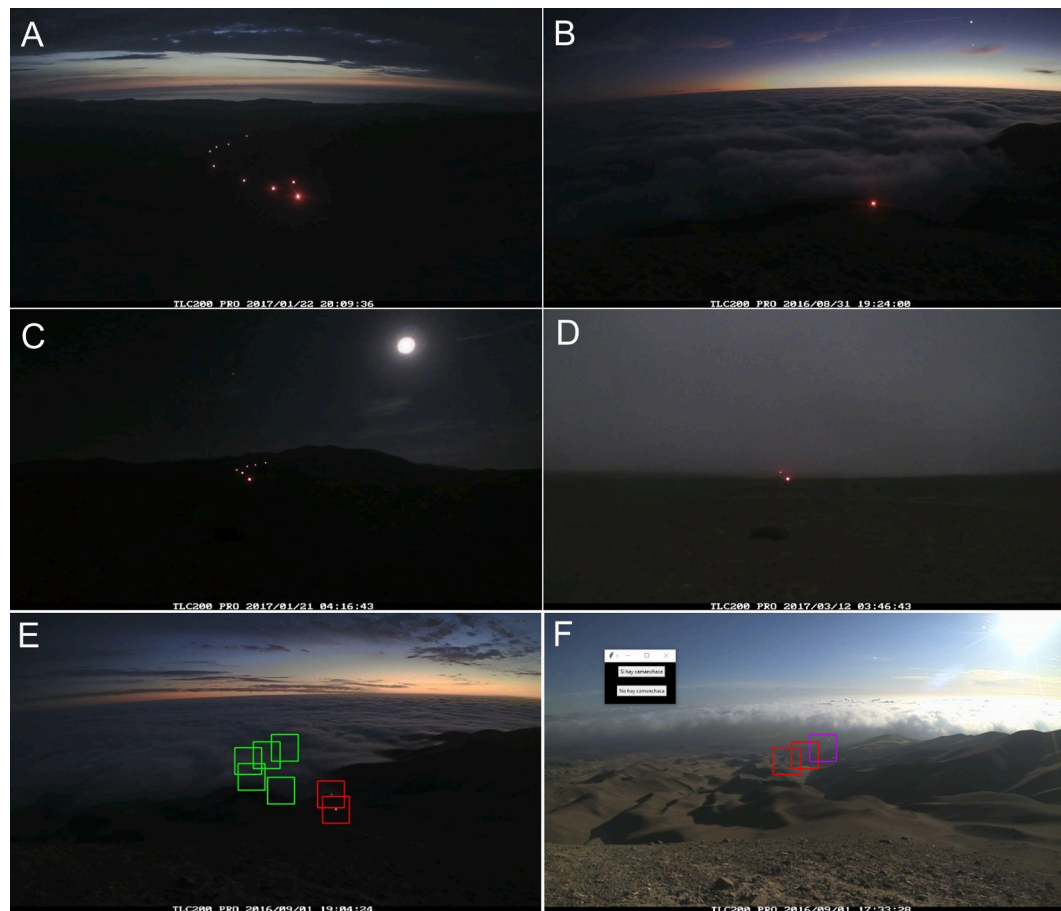
Fig. 2. Example of a GOFOS measurement and the software automatic and manual classifications of ScF. The GOFOS top camera images at 1350 m asl: A) Observation of nine lights, indicating the absence of ScF; B) Observation of one light, indicating fog presence and the CT height (~1200 m asl). The GOFOS bottom camera images at 600 m asl: C) Observation of six lights, indicating the absence of ScF on a full-moon night; D) Observation of two lights, indicating ScF presence and the CB height (700 m asl). GOFOS classification: E) Automatic classification, green squares indicate ScF presence and the red ones indicate its absence; F) Purple square defining ScF presence/absence must be analyzed manually by the user. (For interpretation of the references to colour in this figure legend, the reader is referred to the web version of this article.)

calculated based on the corresponding CB and CT values.

2.3. Supporting data for GOFOS validation

To validate our observations and critically analyze GOFOS performance, we compared its results with datasets (listed and summarized in Table 1) obtained by surface, airborne and satellite observations. In this way, we analyzed GOFOS detections in terms of ScF frequency, CT, and CB.

2.3.1. ScF frequency

As for the fog frequency, GOFOS results were compared with different data derived from surface observations and satellite images (Table 1). For the comparison with surface observations results, we used values of air temperature, relative humidity and air pressure recorded by

two weather stations. The first of these ones is located at 50 m asl at Iquique Airport (20.54917°S, 70.16944°W), and <15 km from the GOFOS. It is administrated by the Meteorological Direction of Chile (DMC) and it has been recording 10-minutes resolution data since 1981 (Fig. 1B). The second fully equipped weather station, operating with the same time resolution, was installed in November 2016 at 1.220 m asl (20.491615°S, 70.058724°W), and <10 km from the GOFOS.

Firstly, we follow the methodology suggested by Lobos et al. (2018), which defines marine boundary layer regimes related to fog formation or dissipation. These regimes are based on a threshold derived from thermal and moisture gradients over a vertical section of the MBL. The reference thresholds for fog formation are 0.0031 K m^{-1} and 0.0016 g kg^{-1} m^{-1}. Thus, we calculated the two marine boundary layer (MBL) fog regimes: well-mixed (fog formation) or stratified (fog dissipation). These results have been modified according to the thresholds derived by

Table 1

Datasets analyzed and compared with GOFOS results.

Analyzed variable	Data type	Source	Analyzed period	Distance to GOFOS location (straight)
ScF Frequency	Surface	Weather stations – Estimation boundary layer regime	2017	15 and 10 km
	Surface	Oktas/Iquique airport	Feb. and Sept. 2017	15 km
	Satellite	GOES image processing	Feb. and Sept. 2017	n/a
Cloud Base	Surface	Ceilometer/Iquique airport	Aug. to Dec. 2017	15 km
	Surfac	Weather stations – Estimation lift condensation level	2017	15 and 10 km
Cloud Top	Airborne	Radiosounding/Antofagasta airport	2017	330 km

GOFOS observations. Using this information, we compared our results for ScF presence with the ones obtained from well-mixed and stratified fog regimes. These regimes are calculated by estimating the potential temperature (θ) and specific humidity (q) from both weather stations over a vertical gradient (from 50 m to 1220 m asl). Subsequently, we calculated the θ and q values per vertical meter. Thanks to this data, we could classify the ABL fog formation (presence) regime (well-mixed) and fog dissipation (absence) regime (stratified) according to:

$$\frac{\partial \overline{\theta}}{\partial z} \approx \frac{\Delta \overline{\theta}}{\Delta z} \begin{cases} < 3.65 \cdot 10^{-3} \text{ K m}^{-1} \text{ Well-mixed} \\ > 3.65 \cdot 10^{-3} \text{ K m}^{-1} \text{ Stratified} \end{cases} \qquad (1)$$

$$\frac{\partial \overline{q}}{\partial z} \approx \frac{\Delta \overline{q}}{\Delta z} \begin{cases} < 1.88 \cdot 10^{-3} \text{ g kg}^{-1} \text{ m}^{-1} \text{ Well-mixed} \\ > 1.88 \cdot 10^{-3} \text{ g kg}^{-1} \text{ m}^{-1} \text{ Stratified} \end{cases} \qquad (2)$$

Secondly, we used another surface observations dataset to validate our results for ScF frequency: the *Oktas* one from Iquique Airport. This dataset is the result of a systematic visual observation performed by an operator of the Airport every hour for the whole year 2017 (these datasets belong to the DMC). To estimate the SCF frequency, we detected fog presence if *Oktas* values were ≥7 (being 8/8 the maximum cloud cover value) in combination with a low cloud condition (CB altitude ≤1500 m asl) recorded by the Oktas operator.

Finally, we compared the ScF frequency obtained by the GOFOS with results derived from Geostationary Operational Environmental Satellite (GOES) images. We calculated the ScF frequency reported by the GOES in February and September 2017, respectively the lowest and highest fog-season month in the coastal Atacama Desert (Cereceda et al., 2008a). For each of these two months, five images per day, captured at 00:39, 04:39, 07:39, 12:39 and 19:39 local time (LT), were processed to represent the fog diurnal-cycle (Farias et al., 2005). As for the nocturnal-cycle, the ScF detection was obtained through a widely used method based on the difference between short (3,8 μm) and long (10,9 μm) thermal infrared wavelengths (Eyre, 1984; Ellrod, 1995; Lee et al., 1997; Anthis and Cracknell, 1999; Bendix, 2002; Underwood et al., 2004; del Río et al., 2018). This method classifies as "low clouds" the pixels presenting both low bright (<-2 μm) and high temperature (>273 K) (Jedlovec and Laws, 2003; Torregrosa et al., 2015). On the other hand, the diurnal ScF identification was based on change detection techniques, contrasting each image with 100% cloud-free ones.

2.3.2. Cloud base

To analyze GOFOS measurements of the CB height, we compared these with two other surface observation data sources (Table 1). The first dataset is obtained by a ceilometer located within Iquique Airport. This instrument, administrated by the DMC, recorded CB values every hour from August to December 2017. The second dataset came from standard meteorological observations taken by the airport weather station, located at 50 m asl. Based on such observations, we applied the methodology suggested by Wetzel and Boone (1995) and already utilized by Lobos et al. (2018) for calculating the lift condensation level (LCL) on the coast of the Atacama Desert. Doing so, we assume the LCL to be the base of the ScF cloud (Lobos et al., 2018).

2.3.3. Cloud top

To validate the CT heights estimated by the GOFOS, we compared these with the radiosoundings' dataset (belonging to DMC) of Cerro Moreno Airport, Antofagasta (23.45361°S, 70.44056°W). These radiosoundings' measurements are taken daily at 12:00 UTC (08:00 local time) ~330 km southern than the GOFOS ones (Fig. 1A). The analysis of this dataset for the whole 2017 revealed a thermal inversion layer height lower than or equal to 1400 m asl.

3. Results and discussions

The advective fog in the Atacama Desert is characterized by ScF

frequency and vertical variability. The complex terrain in which this phenomenon takes place represents a significant variable whose effects are difficult to observe and quantify. Within this context, the GOFOS enables us to describe in-situ ScF variations. In the following section, GOFOS observations regarding ScF frequency, cloud top (CT), cloud base (CB), and cloud depth (CD) are reported.

3.1. ScF frequency according to the GOFOS

GOFOS observations reveal remarkable seasonal and diurnal ScF frequency cycles. The seasonal cycle presents its minimum and its maximum during the austral summer and winter, respectively (Fig. 3A). Fig. 3A shows that the lowest ScF frequencies occur during summer, specifically in January (2% presence) and February (1,5% presence). The ScF frequency starts to escalate fast at the end of autumn, increasing more than double in a month. The highest frequency values occur during winter, in July (49% presence) and August (50% presence). During the southern spring (from September to December), this frequency constantly decreases until the beginning of summer. It is interesting to observe how, even though during spring the fog frequency is not the highest, together with winter, these two seasons correspond to a long fog period covering the second half of the year. Fig. 3B shows ScF diurnal cycle monthly means for representative months (February for summer, May for autumn, August for winter, and November for spring). Within these months, the same diurnal cycles, yet characterized by different magnitudes, are observed.

During the diurnal cycle, the highest ScF frequency occurs during the night (00:00–06:00 LT), the early morning (06:00–09:00 LT) and the evening (19:00–00:00 LT). Conversely, the lowest frequency occurs during the late morning and the afternoon (10:00–18:00 LT). All the reported months, except May, present a fog frequency pick between 20:00 and 22:00 LT. During May, the pick occurs at dawn (06:00–09:00 LT). During February and August, a total absence of fog is reported from the morning to the afternoon. Slightly higher frequency values, ranging from 3 to 5%, are recorded at mid-day (11:00–13:00 LT) in May and in November.

The vertical distribution of the GOFOS along the Coastal Cordillera enables us to quantify the vertical variability of ScF frequency, revealing where fog regularly occurs. Fig. 4 shows the annual ScF frequency vertical variability observed through the GOFOS along the altitudinal pole-lights transect for 2017. We notice that the ScF frequency starts increasing at 600 m asl and reaches its highest value at 1000 m asl. At 1000 m asl, the frequency of ScF starts to decline gradually until 1300 m asl. At 1000 m asl the total annual frequency of ScF is ~30%, consistently with the values represented in Fig. 3. We also noticed that locations below 700 m asl and above 1300 m asl present lower ScF presence (near 10%). At 950 m asl, the increment of ScF frequency presents a discontinuity that might be due to a technical limitation of the GOFOS bottom system (the absence of a light-pole at this height). If so, a ScF frequency between 20 and 25% would be expected at this point.

3.2. Vertical fog distribution

GOFOS observations describe the seasonal diurnal cycles of vertical advective fog distribution. Fig. 5a shows the weekly average seasonal variability of CD, measured from the CT to the CB. These results reveal that the largest CD occurs during summer (~315 m thick), when the CT and CB are at their highest point (Fig. 5a). For example, January, February, and March present average CDs of ~325, ~300, and ~275 m, respectively. This gradual thinning of the CD is mainly due to the decreasing CT height, while the CB one is steady. During autumn, CD values decrease, reaching approximately 230 m, due to both CT and CB height drops. The CD decrease continues during winter (CD = ~220 m), together with the decline of CT and CB values. During this season, the CD reaches its minimum in August (~170 m). Finally, we notice that the spring average CD (~230 m) is slightly higher than the winter one.
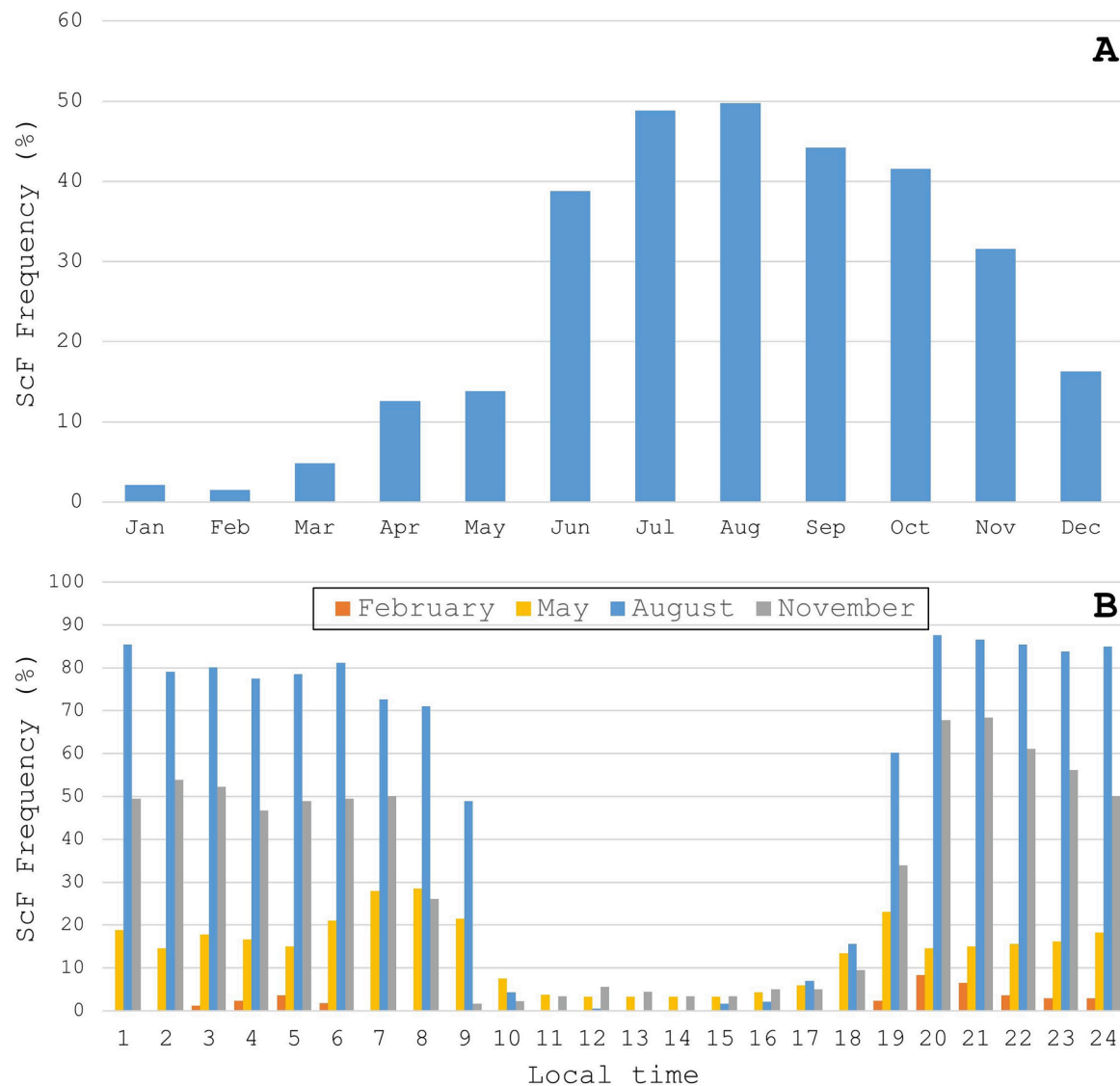
Fig. 3. Fog seasonal and diurnal cycles: A) Monthly ScF frequency in 2017; B) Monthly means of ScF frequency diurnal cycle in February (summer), May (autumn), August (winter), and November (spring).
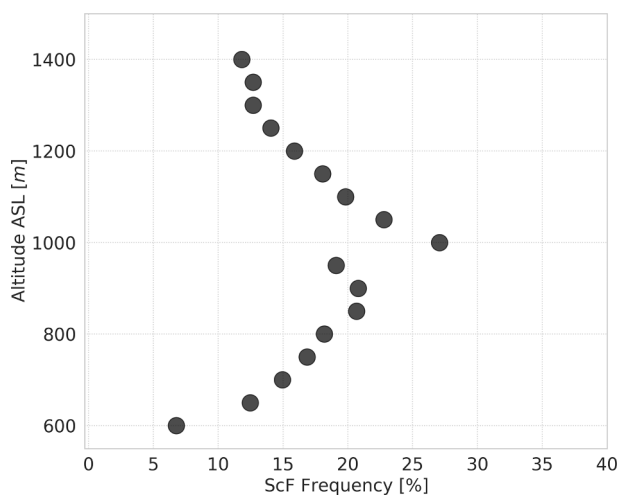

Fig. 4. Annual ScF frequency measured at different heights by the GOFOS in 2017.

Fig. 5b shows the average CD diurnal cycle during January. In the graph, we find some gaps indicating the absence of ScF (Fig. 3A and B). Also, it is possible to observe that the ScF is thicker in the afternoon (i.e. 15:00 LT) than in the morning, while in June the development of the CD diurnal cycle is continuous over the day (Fig. 5c). This is due to the rapid ScF rise occurring between 13:00 and 14:00 LT, followed by a progressive decrease until midnight (20:00–24:00 LT). Finally, during November (Fig. 5d), a continuous ScF increase can be observed, with the highest CD (~400 m) reached during the afternoon (14:00–18:00 LT).

Fig. 6a shows the inverse relationship between CT diurnal cycle and fog frequency: the lower (higher) the CT height, the higher (lower) the ScF frequency. It is relevant to note that the highest recorded CT values is ~1000 m of height, consistently with the data showed in Fig. 4. As for the annual negative correlation between CT and ScF frequency (Fig. 6a), the R^2 of 0.40, ($p < 0.005$) increases until 0.60 ($p < 0.005$) if summer months are excluded from the analysis. Fig. 6a also shows that the highest ScF frequencies correspond to the lowest CT heights (between 900 and 1100 m asl) and that these frequencies increase mainly during the night, when the CT is shallower. Conversely, the lowest ScF presence occurs between noon and the afternoon, consistently with its diurnal cycle presented in Fig. 3b. On the other hand, Fig. 6b shows a low correspondence between the CB height and the ScF frequency. This
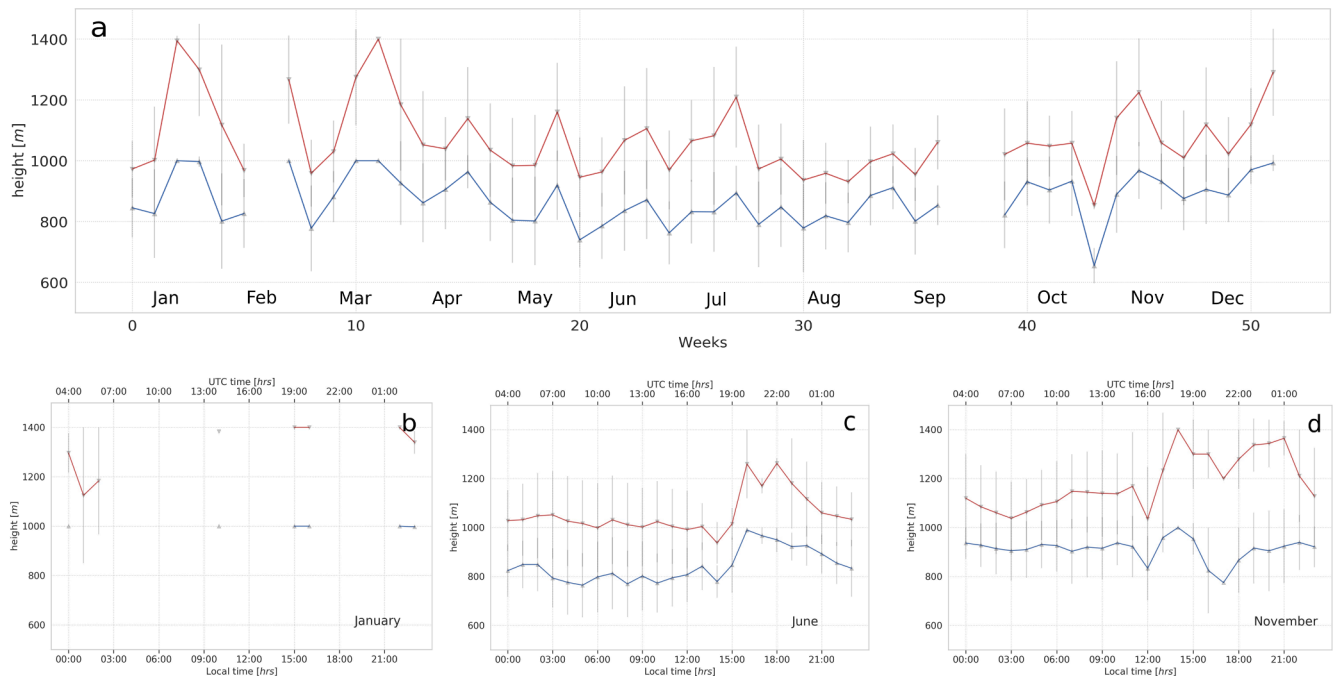
Fig. 5. Monthly and diurnal CD cycles in 2017, defined through the CT (red lines) and CB (blue lines) levels. Grey vertical lines show CT and CB maximum and minimum values: a) CD weekly averages in 2017; b), c) and d) show the CD diurnal cycle in January, June, and November, respectively. (For interpretation of the references to colour in this figure legend, the reader is referred to the web version of this article.)
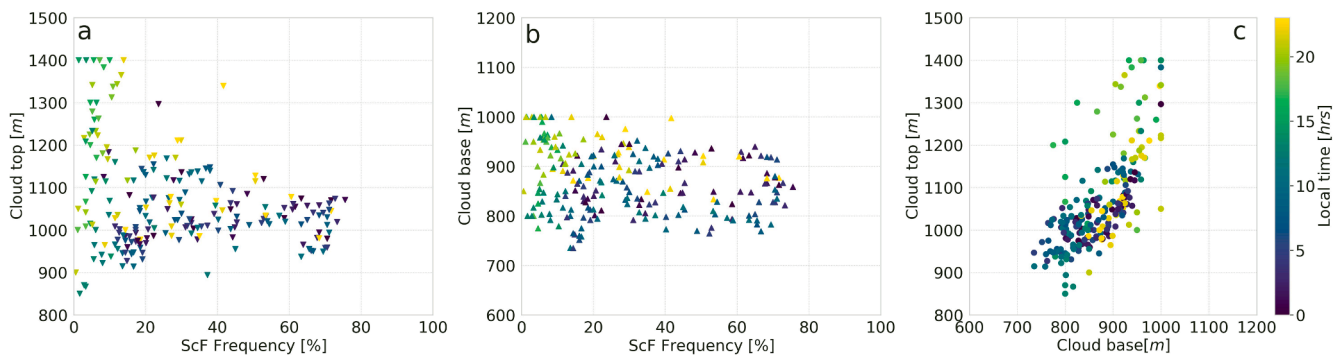
Fig. 6. Correlation between the diurnal cycle annual averages of: a) ScF frequency and CT height; b) ScF Frequency and CB height; and c) CT and CB heights.

means that these two variables are mainly independent of each other. Nevertheless, as for the ScF diurnal cycle, we can observe that the CB one has a similar trend to the CT one (Fig. 6a and b), where the highest (lowest) frequency of ScF presence occurs during the night and the morning (noon-afternoon). Fig. 6c shows a positive correlation between the CT and CB height values. The highest correspondence between these two variables occurs during the night and at dawn, when ScF regularly forms with CT at 1000 m of height and CB at ~850 m of height. The annual correlation between CT and CB values is characterized by an R^2 of 0.44 ($p < 0.005$), while the monthly analysis report that 75% of the analyzed months present an R^2 of 0.77 ($p < 0.005$), revealing a strong correlation between these variables.

## 4. GOFOS and the standard stratocumulus and fog observations methods

Within this section, we compare GOFOS observations of Stratocumulus-fog (ScF) frequency, cloud base (CB), and cloud top (CT) with the ones obtained through the standard methods introduced in Section 2.3 and listed in Table 1.

4.1. ScF frequency observed by the GOFOS and standard methods

4.1.1. The atmospheric boundary layer regimes

We compared GOFOS observations of the ScF frequency with the estimations of fog formation (presence) and dissipation (absence) classified through the marine boundary layer (MBL) regimes method by Lobos et al. (2018) (Section 2.3, Eqs. (1) and (2)). For performing this comparison, we only analyzed fog presence events whose CT is at least at 1220 m asl because the MBL regimes method requires the presence of weather stations below the CT for correct fog classification. The ScF presence observed through the GOFOS (467 total hours in 2017) 87% corresponds with an MBL under moisture (q) well-mixed regime, whereas the correspondence decreases to 79% considering an MBL regime under thermal well-mixed conditions. We hypothesize that the higher agreement between GOFOS ScF frequency observations and the (q)-well-mixed regime is due to the direct relationship existing between q and the fog. The high consistency between GOFOS results and both (θ) and (q) well-mixed regimes, indicates that ScF has a high possibility (>80%) to form when q and θ within the MBL are lower than 1,88 g kg^{-1} and 3.65 K, respectively. Yet, we observe seasonal and diurnal variabilities of these results. Fig. 7 shows the distribution of the analyzed
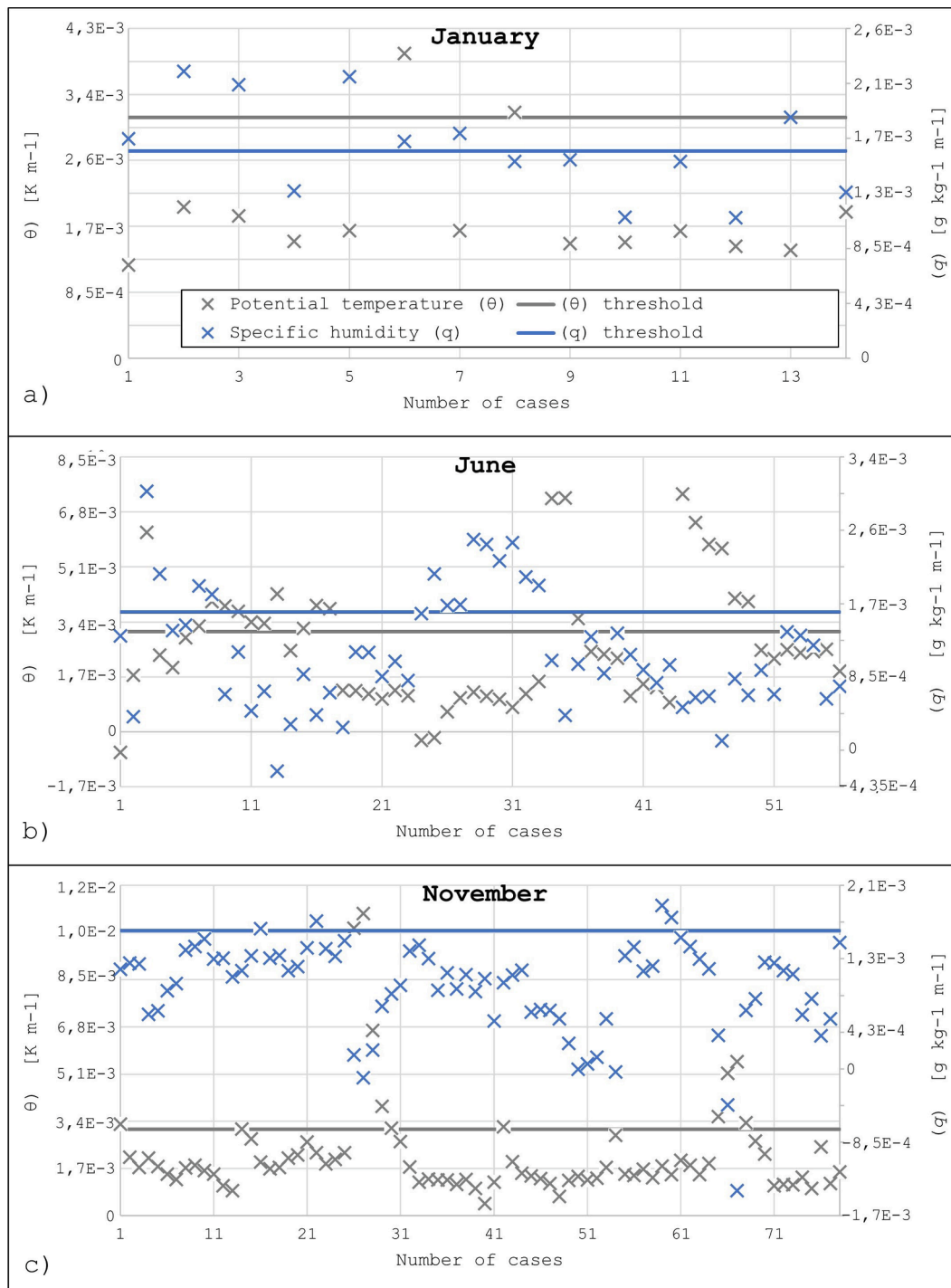
Fig. 7. January, June and November variability of the agreement between GOFOS results and the well-mixed MBL regimes. Crosses indicate the observed cases of q-well-mixed (blue) and θ-well-mixed (grey) regimes. Blue and grey lines define the difference between well-mixed regimes (under the line) and the stratified ones (above the line). (For interpretation of the references to colour in this figure legend, the reader is referred to the web version of this article.)

cases of both ScF frequency and MBL regimes for January, June, and November, representative months for summer, winter and spring, respectively. On one hand, analyzing January data (Fig. 7a), we notice that 12 out of the 14 cases present a correspondence between θ-well-mixed regimes and ScF frequency, reaching an 85% agreement between these two datasets. On the other hand, the results reveal a 50% consistency between the q-well-mixed regime and ScF frequency. As for June (Fig. 7b), the agreement between θ well-mixed regime and ScF frequency decreases to 64%, whereas a 77% consistency with q-well-mixed regimes is found. Finally, in November (Fig. 7c), both well-mixed

regimes reach their highest agreement with GOFOS ScF frequency observations: 95% for the q-well-mixed regime and 85% for the θ-well-mixed regime.

As for the diurnal variabilities of well-mixed regimes and GOFOS observations, Table 2 shows their average agreement for January, June, and November. In general, high correspondence is found during the evening-night transition, where GOFOS results are more consistent with q-well-mixed regimes than with the θ-well-mixed ones. Data related to January 2017 show less ScF presence, together with a significant correspondence between the MBL regimes method and GOFOS

Table 2

Diurnal distribution of the agreement between GOFOS observations and well-mixed regimes for January, June, and November 2017. Columns show the number of the total analyzed cases of correspondence between GOFOS results and θ-well-mixed and q-well-mixed regimes.

Local time	Number of agreement								
	January			June			November		
	N° of cases	(θ)	(q)	N° of cases	(θ)	(q)	N° of cases	(θ)	(q)
1	0	0	0	4	3	2	3	3	2
2	0	0	0	4	3	2	4	4	4
3	0	0	0	1	1	0	5	5	5
4	0	0	0	3	3	2	6	6	6
5	0	0	0	3	3	2	7	7	7
6	0	0	0	2	2	1	6	6	6
7	1	1	0	2	2	1	5	5	5
8	0	0	0	1	1	0	2	2	2
9	0	0	0	2	1	1	0	0	0
10	0	0	0	2	1	2	1	0	1
11	0	0	0	0	0	0	1	0	1
12	0	0	0	1	0	1	1	0	1
13	1	0	0	2	0	2	1	0	1
14	0	0	0	1	0	1	1	0	1
15	0	0	0	2	0	2	0	0	0
16	0	0	0	2	0	2	0	0	0
17	0	0	0	3	2	3	0	0	0
18	0	0	0	3	1	3	2	0	2
19	2	1	1	3	1	2	6	3	6
20	7	7	3	1	0	1	8	6	8
21	2	2	2	2	1	2	8	8	7
22	1	1	1	4	3	3	4	4	4
23	0	0	0	4	4	4	4	4	3
24	0	0	0	4	4	4	3	3	2
Total	14	12	7	56	36	43	78	66	74

Table 3

Comparison of results for ScF frequency obtained by GOES, GOFOS, and *Oktas* datasets during February and September 2017.

Stratocumulus or fog cloud monthly frequency (%)								
Mean	GOES over GOFOS area		GOFOS		GOES over airport area		Airport (oktas)	
	Feb	Sep	Feb	Sep	Feb	Sep	Feb	Sep
Monthly	1,5	41	1,5	44	0,7	52	1,6	56,3
0:39	3	58	3	68	3	71	3	73
4:39	3	56	3	63	3	68	3	70
7:39	3	56	0	58	0	68	3	70
12:39	0	7	0	7	0	29	0	40
19:39	0	28	3	49	0	23	0	30

observations. In June, the MBL regimes method reports higher daily ScF presence and lower agreement with GOFOS observations. Finally, in November the MBL regimes technique shows the highest ScF presence and the best correspondence with GOFOS dataset. These results are consistent with the ones obtained by Lobos et al. (2018) over the same study area during 2015.

4.1.2. Satellite dataset and Oktas observations

The ScF presence measured by the GOFOS was compared with the ones recorded through GOES satellite datasets and *Oktas* observations from Iquique Airport. The processed GOES images define ScF frequency within the study area over the GOFOS and *Oktas* working ranges, which correspond to one GOES cell size (pixel of 1–4 km). As for the O*ktas* dataset, we considered observations reporting a cloud cover ≥7 to correspond to ScF presence. We performed two different kinds of comparisons between February and September monthly averages of the ScF frequency. To estimate these averages, we analyzed five images per day taken by the GOES (at 0:39, 04:39, 07:39, 12:39, 19:39 local time), GOFOS measurements taken every 10 min, and *Oktas* hourly observations. Firstly, we correlated the results obtained by GOES with the ones derived by the GOFOS. Secondly, we compared *Oktas* and GOES monthly means for each of the five GOES images, for the corresponding 5 moments of the day. Table 3 shows monthly ScF frequency means estimated by GOES for the two study fields: over the GOFOS installation and in the Iquique airport area. During September, GOES results show slightly less ScF frequency than GOFOS and *Oktas* measurements, reaching a ~93% agreement with these two. Even though GOFOS and *Oktas* monthly mean estimations are based on significantly more data, the analysis of satellite images at selected hours represents an effective method for describing the monthly ScF frequency. As for the monthly average diurnal cycles, the highest difference between GOES and GOFOS results occurs at sunset. Nevertheless, the observations taken during the rest of the day show a high agreement among these two datasets, reaching a 100% correspondence at noon. Also, comparing results

obtained by GOES and the *Oktas*, we find high agreement among these two at night (nearly 100% agreement), but such correspondence decreases at noon and sunset. The comparison between GOFOS and *Oktas* results shows that the *Oktas* detected a higher ScF frequency both as monthly and daily averages, except for the measurements taken at sunset. The higher ScF frequency shown by the *Oktas* may be due to the location from which the two measurements were taken since Iquique Airport is located on the coastal plain (3 km from the coastline), where oceanic conditions dominate and the land heat influence is lower. On the other hand, the GOFOS is located over the Coastal Cordillera (15–20 Km onshore), where the topography and the land heating significantly influence the dissipation of the fog (Lobos et al., 2018). The ScF diurnal cycles defined by Oktas and GOFOS observations reveal the described geographic influence showing similar percentages of ScF frequency at night and dawn. Such results are associated with ScF inland advection events (Farías et al., 2005). Conversely, the biggest difference between observations obtained through these two methods occurs at noon, when solar radiation dissipates the ScF. As for February 2017, the comparison between GOFOS, *Oktas*, and GOES results should be interpreted cautiously, due to a low ScF frequency within the study area. Yet, ScF presence monthly means show a strong agreement between GOES and GOFOS results since both datasets report a 1,5% of ScF frequency for this month. As for the comparison between GOES and O*ktas* results, the ScF frequency reported by GOES is about 50% lower than the one obtained by the Oktas measurements (Table 3). As for ScF frequency monthly hourly means, GOES shows a similar level of agreement with both GOFOS and *Oktas* values since observations obtained through these last two techniques present identical ScF frequencies at night and different ones at dawn, noon, and sunset.

GOFOS and *Oktas* measurements provide a site-specific estimation of ScF presence. The precision of the results obtained through these techniques would be difficult to equal through satellite data sources. Yet, satellite datasets allow us to monitor and understand the spatiotemporal dynamics of the ScF phenomenon.

4.2. Cloud base observed through the GOFOS and surface observations

Within this section, we compare CB values obtained by the GOFOS with the ones obtained through two other techniques: the ceilometer and the lift condensation level (LCL) method.

Firstly, we compare our CB results with measurements taken by a ceilometer in the Airport of Iquique. Secondly, we use meteorological data provided by Iquique Airport to estimate the LCL (Wetzel and Boone, 1995), assuming it to correspond to the base of stratocumulus clouds (section 2.3). Fig. 8 shows boxplots of the CB height monthly means derived by both GOFOS and ceilometer results from August to December 2017. We found an expected positive correlation between both datasets (r = +0.6, 95% confidence level). Yet, this analysis shows how the CB height indicated by the GOFOS is on average ~80 m higher than the one measured by the ceilometer. Such a difference might be due to topographic reasons since the mountain barrier present in the study area
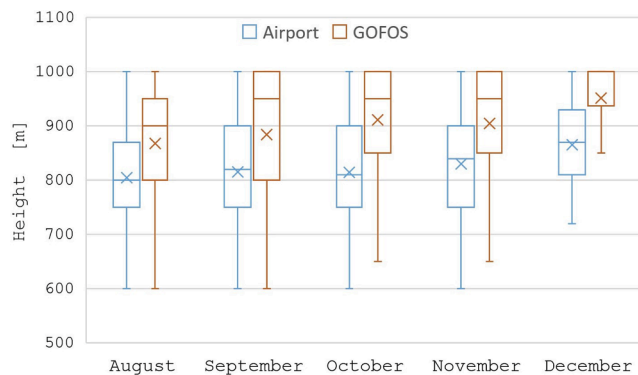
Fig. 8. Comparison between monthly CB heights measured by Iquique Airport ceilometer and the GOFOS from August to December 2017.

forces the ScF to rise (Cereceda et al., 2008b).

As for the comparison between the CB values estimated through the LCL method (CB_{LCL}) and the ones described by the GOFOS (CB_{GOFOS}), we generally observe lower CB_{LCL}. These results are shown in Fig. 9, together with a comparison between CT measurements obtained by the GOFOS and by the Antofagasta Airport radiosounding. This comparison is analyzed in the next section. Moreover, Table 4 summarizes the descriptive statistics related to the comparison shown in Fig. 9. The mean CB values observed by the GOFOS differ only by 7% from the CB values estimated through the LCL methods, being the CB_{GOFOS} higher than the CB_{LCL} (Table 4). This difference is due to the influence that topography exerts over the CB, rising its value (Fig. 1B). Also, both these methods report similar standard deviations (76 m for GOFOS results and 80 m for the ones obtained through the LCL method). Comparing the CB extreme values derived from the two datasets, we observe that the maximum CB height detected through both methods almost coincide, while minimum values differ by 9% from each other. Finally, analyzing the interquartile area (25%, 50%, and 75%), we observe large differences of ~100 m, probably caused by the seasonal ScF variability affecting both methods.

4.3. Cloud top observed by the GOFOS and radiosounding

Finally, we compared CT observations derived from the GOFOS (CT_{GOFOS}) with the ones obtained by the Antofagasta Airport radiosoundings (CT_{RS}). This comparison is shown in Fig. 9 (and summarized in Table 4), where it is possible to observe that the CT_{GOFOS} mean is ~80 m higher than the CT_{RS} one. To analyze this mismatch, three factors are
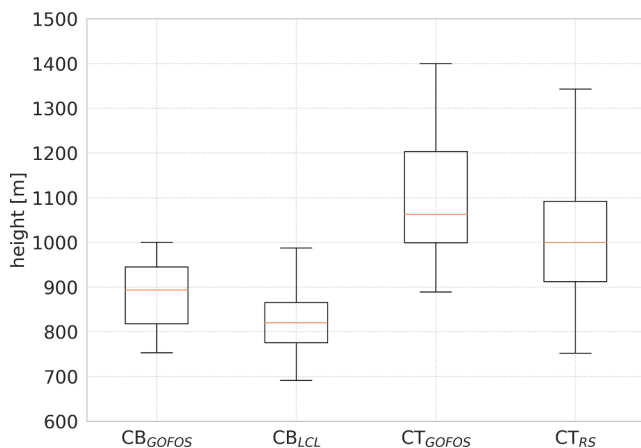
Fig. 9. Annual means of CB and CT heights observed by the GOFOS, CB annual mean height determined by the LCL method, and CT annual mean height measured through radiosoundings (RS).

Table 4

Descriptive statistics of CB measurements obtained by the GOFOS and by the LCL method, and CT values observed by the GOFOS and by Antofagasta Airport radiosounding during 2017.

	CB GOFOS	CB-LCL	CT-GOFOS	CT-Radiosounding
Mean	888.40	828.89	1107.71	1022.09
Std	76.29	80.10	143.13	158.26
Min	753.20	691.22	888.88	752.00
25%	817.89	775.46	999.29	912.00
50%	893.69	820.35	1062.66	1000.00
75%	945.00	865.40	1203.51	1092.00
Max	1000.00	1075.59	1400.00	1500.00

taken into account. Firstly, we have to carefully take into consideration the different latitudes of the two observation points (the GOFOS one is approximately 330 km further N than the Antofagasta Airport), and the annual displacement of the SE Pacific anticyclone, which causes an increase of the CT height from S to N (Garreaud et al., 2008). However, we believe that no significant differences are generated by the latitudinal variation since both locations present similar synoptic and geographical conditions. Secondly, RS are launched from the coastal plain, while GOFOS measurements are taken from the coastal Cordillera, where local topography influences the CT height. Thirdly, the difference between observation times plays a significant role in determining the contrast between CT_{GOFO} and CT_{RS} values since CT_{GOFOS} results are based on observations taken for all hours of fog events, whereas CT_{RS} values are based on 08:00 LT measurements only, when the boundary layer is likely to be shallow.

It is possible to conclude that higher CT_{GOFOS} values are justified by the influence of topography.

Moreover, comparing CT mean heights obtained through these two methods, we notice about an 8% difference among their results. The standard deviation of both methods is also similar: analyzing their extreme values, it emerges that the respective CTs differ of maximum 100 m and minimum ~30 m between GOFOS and RS results. Finally, the trends shown within the interquartile area are consistent with these observations (~60–100 m).

5. Conclusions

In this paper, we present the GOFOS as a new method for describing fog frequency and vertical distribution, combining the advantages of high temporal resolution of surface observations with the ones given by the peculiar geography of the coastal Atacama Desert.

This technique characterizes the vertical elevation range of the stratocumulus cloud providing direct observations of the advective fog presence, the height of the cloud base (CB) and the one of the cloud top (CT). Such information allows us for the first time to characterize in-situ the vertical distribution of the ScF phenomenon.

A high agreement was found between GOFOS fog frequency results and the ones measured through standard methods, reaching ~93% correspondence between GOFOS and GOES datasets. Likewise, there is a consistency between GOFOS observations and the ones obtained through the marine boundary layer (MBL) regimes method for studying fog formation and dissipation. This agreement reaches 87% when comparing observations made by the GOFOS with specific humidity well-mixed regimes. On the other hand, GOFOS results are 79% consistent with potential temperature well-mixed regimes. This two-ways validation may be further explored to improve the MBL regimes method for obtaining a better classification of the ScF formation or dissipation.

The GOFOS is also presented as a reliable method for determining vertical ScF cloud variability by setting the highest fog frequency at ~1000 m asl. This frequency is consistent with the highest CT and the thinnest CD means during the fog season (June-November). As for the CB, this maintains a steady-state along the annual cycle. On the other

hand, CB is significantly variable within its diurnal-cycle, where the highest ScF frequency occurs during the night and morning and the lowest ScF frequency occurs during the noon and afternoon, in agreement with the highest ĆTs observations. GOFOS observations of ScF vertical distribution demonstrated to be consistent with results obtained by more commonly used methods. Finally, the GOFOS can well-describe the influence of topography on ScF dynamics.

Nevertheless, this method presents some uncertainties. Firstly, only the clouds located within GOFOS installation range can be analyzed. This limited coverage reduces the capacity of observation of the method. Secondly, a better description of the ScF vertical variability would be obtained through a higher resolution than the one provided by the GOFOS (50 m vertical resolution). Thirdly, the GOFOS location, which significantly influences its results through topography and slope orientation, might be considered as an exceptional one. Finally, long-term measurements (>5 years) would allow validating GOFOS results based on longer time-series of data. This would allow analyzing GOFOS performance in representing larger-scale phenomena (e.g., the ENSO phases). Moreover, given the distance between the camera and the pole-lights, there might be a lag in the measurement." Despite these uncertainties, the GOFOS was revealed to be a simple, reliable, and affordable technique. Thus, this method represents a good alternative for the systematic and automatic monitoring of fog presence and its vertical distribution. Moreover, the GOFOS can be adapted and improved for different topographic conditions.

Potentials and projections related to this new method are described below:

- The GOFOS allows us to better understand the relationship between ScF vertical structure and frequency. These data are useful to qualify potential areas for fog harvesting.
- The GOFOS provides the possibility to relate ScF vertical distribution to spatial changes in fog-dependent ecosystems. This knowledge significantly contributes to the study of the relationship between atmosphere and biosphere for better understanding past and future climatic changes.
- The GOFOS contributes to the validation of other methodologies, such as the MBL regimes method, for classifying fog formation and dissipation, two key variables for fog forecasting.
- The GOFOS contributes to the validation of satellite datasets, adding ground truth to the ScF identification and characterization process.
- Local-scale datasets (provided by the GOFOS and the weather stations) significantly contribute to our understanding of the physics of cloud formation. These results could be improved by adding to the GOFOS installation more sensors measuring additional atmospheric variables such as temperature, relative humidity, wind speed, and air pressure. Through this upgrade, the GOFOS could better characterize the thermodynamics of the ScF vertical profile, providing fundamental knowledge for the understanding of fog presence and its physical characteristics, such as its liquid water content.

CRediT authorship contribution statement

Camilo del Río: . **Felipe Lobos:** Conceptualization, Formal analysis, Investigation. **Alexander Siegmund:** Supervision, Conceptualization. **Cristian Tejos:** Methodology, Software. **Pablo Osses:** Investigation. **Zeidy Huaman:** Investigation. **Juan Pablo Meneses:** Software. **Juan-Luis García:** Investigation. All authors helped writing the paper.

Declaration of Competing Interest

The authors declare that they have no known competing financial interests or personal relationships that could have appeared to influence the work reported in this paper.

References

Anthis, A., Cracknell, A.P., 1999. Use of satellite images for fog detection (AVHRR) and forecast of fog dissipation (METEOSAT) over lowland Thessalia. Hellas. Int. J. Remote Sens. 20, 1107–1124.

Bendix, J., 2002. A satellite-based climatology of fog and low level stratus in Germany and adjacent areas. J. Atmos. Res. 64, 3–18.

Bendix, J., Thies, J., Cermak, J., Nauss, T., 2005. Ground fog detection from space on MODIS daytime data – a feasible study. Weather Forecast. 20, 989–1005.

Bretherton, C.S., Wood, R., George, R.C., Leon, D., Allen, G., Zheng, X., 2010. Southeast pacific stratocumulus clouds, precipitation and boundary layer structure sampled along 20° S during VOCALS-Rex. J. Atmos. Chem. Phys. 10, 10639–10654.

Bruijnzeel, L.A., Eugster, W., Burkard, R., 2005. Fog as a hydrologic input. In: Anderson, M.G., McDonnell, J.J. (Eds.), Encyclopedia of Hydrological Sciences, vol. 1, Chichester et al., pp. 559–582.

Cereceda, P., Osses, P., Larrain, H., Farías, M., Pinto, R., Schemenauer, R.S., 2002. Advective, orographic and radiation fog in the Tarapacá region, Chile. J. Atmos. Res. 64, 261–271.

Cereceda, P., Larrain, H., Osses, P., Farías, M., Egaña, I., 2008a. The spatial and temporal variability of fog and its relation to fog oases in the Atacama Desert, Chile. J. Atmos. Res. 87, 312–323.

Cereceda, P., Larrain, H., Osses, P., Farías, M., Egaña, I., 2008b. The climate of the coast and fog zone in the Tarapacá Region, Atacama Desert, Chile. J. Atmos. Res. 87, 301–311.

Cermark, J., 2007. SOFOS – A new Sattelite-based Operational Fog Observation Scheme. Marburg/Lahn: Marburger Geographische Ges.XIX, 132 S graph. Darst., Kt.

del Río, C., Garcia, J.-L., Osses, P., Zanetta, N., Lambert, F., Rivera, D., Siegmund, A., Wolf, N., Cereceda, P., Larraín, H., Lobos, F., 2018. ENSO influence on coastal fog-water yield in the Atacama Desert, Chile. Aerosol Air Qual. Res. 18 (1), 127–144.

Duynkerke, P.G., Zhang, H.Q., Jonker, P.J., 1995. Microphysical and turbulent structure of nocturnal stratocumulus as observed during ASTEX. J. Atmos. Sci. 52 (16), 2763–2777.

Ellrod, G., 1995. Advances in the detection and analysis of fog at night using GOES multispectral infrared imagery. Weather Forecast. 10, 606–619.

Eugster, W., 2008. Fog research. Die Erde 139 (1–2), 1–10.

Eyre, J.R., 1984. Detection of fog at night using Advanced Resolution Radiometer (AVHRR) imagery. Meteorol. Mag. 113, 266–271.

Farías, M., Cereceda, P., Osses, P., Larraín, H., 2005. Comportamiento espacio temporal de la nube estratocúmulo, productora de niebla en la costa del desierto de Atacama (21° lat. S., 70° long W.) durante un mes de invierno y otro de verano. Invest. Geog. 56, 43–61.

Garreaud, R., Muñoz, R., 2004. The diurnal cycle of circulation and cloudiness over the subtropical southeast Pacific: a modelling study. J. Clim. 17, 1699–1710.

Garreaud, R., Barichivich, J., Christie, D., Maldonado, A., 2008. Interannual variability of the coastal fog at Fray Jorge relicts forests in semiarid Chile. J. Geophys. Res. 113, G04011.

Garreaud, R.D., Rutllant, J.A., Muñoz, R.C., Rahn, D.A., Ramos, M., Figueroa, D., 2011. VOCALS-CUpEx: the Chilean upwelling experiment. Atmos. Chem. Phys. 11 (5), 2015–2029.

Gultepe, I., Tardif, R., Michaelides, S.C., Cermak, J., Bott, A., Bendix, J., Müller, M.D., Pagowski, M., Hansen, B., Ellrod, G., Jacobs, W., Toth, G., Cober, S.G., 2007. Fog research: a review of past achievements and future perspectives. Pure Appl. Geophys. 164, 1121–1159. https://doi.org/10.1007/s00024-007-0211-x.

Jedlovec, G.J., Laws, K., 2003. GOES cloud detection at the Global Hydrology and Climate Center. Paper P1 presented at 12th conference on satellite meteorology and oceanography, Am. Meteorol. Soc., Long Beach, Canada, Feb.

Klemm, O., Schemenauer, R.S., Lummerich, A., Cereceda, P., Marzol, V., Corell, D., van Heerden, J., Reinhard, D., Gherezghiher, T., Olivier, J., Osses, P., Sarsour, J., Frost, E., Estrela, M.J., Valiente, J.A., Fessehaye, G.M., 2012. Fog as a fresh-water resource: overview and perspectives. Ambio 41 (3), 221–234.

Koch, M.A., Kleinpeter, D., Auer, E., Siegmund, A., del Rio, C., Osses, P., García, J.-L., Marzol, M.V., Zizka, G., Kiefer, C., 2019. Living at the dry limits: ecological genetics of Tillandsia landbeckii lomas in the Chilean Atacama Desert. Plant Systemat. Evol. 305 (10), 1041–1053.

Larraín, H., Velásquez, F., Cereceda, P., Espejo, R., Pinto, R., Osses, P., Schemenauer, R. S., 2002. Fog measurements at the site "Falda Verde" north of Chañaral compared with other fog stations of Chile. J. Atmos. Res. 64, 273–284.

Latorre, C., González, A.L., Quade, J., Fariña, J.M., Pinto, R., Marquet, P.A., 2011. Establishment and formation of fog-dependent Tillandsia landbeckii dunes in the Atacama Desert: evidence from radiocarbon and stable isotopes. J. Geophys. Res. 116, G03033.

Lee, T., Turk, J., Richardson, K., 1997. Stratus and fog products using GOES-8-9 3.9 μm Data. Weather Forecast. 12, 664–677.

Liu, Y., Racah, E., Correa, J., Khosrowshahi, A., Lavers, D., Kunkel, K., … Collins, W., 2016. Application of deep convolutional neural networks for detecting extreme weather in climate datasets. arXiv preprint arXiv:1605.01156.

Lobos, F., Vilà-Guerau, J., Pedruzo-Bagazgoitia, X., 2018. Characterizing the influence of the marine stratocumulus cloud on the land fog at the Atacama Desert. J. Atmos. Res. 214, 109–120.

Marzol, M.V., 2002. Fog water collection in a rural park in the Canary Islands (Spain). J. Atmos. Res. 64, 239–250.

Marzol, M.V., 2005. La captación del agua de la niebla en la isla de Tenerife. Ed. Caja de Canarias, 220p. Islas Canarias, España.

Marzol, M.V., Sánchez, J., 2008. Fog water harvesting in Ifni, Morocco. An assessment of potential and demand. Die Erde 139, 97–126.

Muñoz, R., Zamora, R., Rutllant, J., 2011. The coastal boundary layer at the eastern Margin of the southeast Pacific (23.4 degrees S, 70.4 degrees W): cloudiness-conditioned climatology. J. Clim. 24, 1013–1033.

Muñoz, R., Quintana, J., Falvey, M., Rutllant, J., Garreaud, R., 2016. Coastal clouds at the eastern Margin of the southeast Pacific: climatology and trends. J. Clim. 29, 4525–4542.

Muñoz-Schick, M., Pinto, R., Mesa, A., 2001. Oasis de neblina en los cerros costeros del sur de Iquique, región de Tarapacá, Chile, durante el evento El Niño 1997–1998. Rev. Chil. Hist. Nat. 74, 389–405.

Pinto, R., Barria, I., Marquet, P.A., 2006. Geographical distribution of Tillandsia lomas in the Atacama Desert, northern Chile. J. Arid Environ. 65, 543–552.

Roach, W.T., Brown, R., Caughey, S.J., Garland, J.A., Readings, C.J., 1976. The physics of radiation fog: I – a field study. Quart. J. Roy. Meteorol. Soc. 102, 313–333.

Roach, W.T., 1994. Back to basics: fog: Part 1 – Definition and basic physics. Weather 49, 411–415.

Rutllant, J., Fuenzalida, H., Aceituno, P., 2003. Climate dynamics along the arid northern coast of Chile: The 1997–1998 Dinámica del Clima de la Región de Antofagasta (DICLIMA) experiment. J. Geophys. Res. 108, 4538.

Rutllant, J., Garreaud, R., 2005. Capa límite marina en el Pacífico suroriental subtropical durante el Crucero CIMAR-5. Revista Chilena de Ciencia y Tecnología del Mar, 28 (1), 25–33.

Schemenauer, R.S., Joe, P.I., 1989. The collection efficiency of a massive fog collector. Atmos. Res. 24(1–4), 53–69.

Schemenauer, R.S., Cereceda, P., 1994a. A proposed standard fog collector for use in high elevation regions. J. Appl. Meteorol. 33 (11), 1313–1322.

Schemenauer, R.S., Cereceda, P., 1994b. Fog collection's role in water planning for developing countries. Nat. Resour. Forum 18(2), 91–100. https://doi.org/10.1111/j.1477-8947.1994.tb00879.x.

Schulz, N., Aceituno, P., Richter, M., 2011a. Phytogeographic divisions, climate change and plant dieback along the coastal desert of northern Chile. Erdkunde 65 (2), 169–187.

Schulz, N., Boisier, J.P., Aceituno, P., 2012. Climate change along the arid coast of northern Chile. J. Clim. 32 (12), 1803–1814.

Schween, J., Hoffmeister, D., Löhnert, U., 2020. Filling the observational gap in the Atacama Desert with a new network of climate stations. Global Planet. Change 184, 103034.

Serpetzoglou, E., Albrecht, B.A., Kollias, P., Fairall, C., 2008. Boundary layer, cloud, and drizzle variability in the southeast Pacific stratocumulus regime. J. Clim. 21, 6191–6214.

Shi, M., Xie, F., Zi, Y., Yin, J., 2016. Cloud detection of remote sensing images by deep learning. In: 2016 IEEE International Geoscience and Remote Sensing Symposium (IGARSS), IEEE, pp. 701–704.

Stull, R., 1988. In: An Introduction to Boundary Layer Meteorology. Kluwer Academic Publishers, The Netherlands, p. 670.

Torregrosa, A., Combs, C., Peters, J., 2015. GOES-derived fog and low cloud indices for coastal north and central California ecological analyses. Earth Space Sci. 3, 46–67.

Underwood, J., Ellrod, G., Kuhnert, A., 2004. A multiple-case analysis of nocturnal radiation-fog development in the central valley of California utilizing the GOES nighttime fog product. J. Appl. Meteorol. 43, 297–311.

Wetzel, P.J., Boone, A., 1995. A Parameterization for Land–Atmosphere-Cloud Exchange (PLACE): documentation and testing of a detailed process model of the partly cloudy boundary layer over heterogeneous land. J. Clim. 8 (7), 1810–1837.

Zhang, J., Liu, P., Zhang, F., Song, Q., 2018. CloudNet: Ground-based cloud classification with deep convolutional neural network. Geophys. Res. Lett. 45 (16), 8665–8672.